

MIPS is a Maxwell fluid with an extended and non-monotonic crossover

José Martín-Roca and Chantal Valeriani*

Dept. de Estructura de la Materia, Física Térmica y Electrónica, Universidad Complutense de Madrid, Spain

Kristian Thijssen

Niels Bohr Institute, University of Copenhagen, Denmark

Tyler Shendruk[†]

School of Physics and Astronomy, University of Edinburgh, UK

Angelo Cacciuto[‡]

Department of Chemistry, Columbia University, New York, USA

Understanding the mechanical properties of active suspensions is crucial for their potential applications in materials engineering. Among the various phenomena in active matter that have no analogue in equilibrium systems, motility-induced phase separation (MIPS) in active colloidal suspensions is one of the most extensively studied. However, the mechanical properties of this fundamental active state of matter remain poorly understood. This study investigates the rheology of a suspension of active colloidal particles under constant and oscillatory shear. Systems consisting of pseudo-hard active Brownian particles exhibiting co-existence of dense and dilute phases behave as a viscoelastic Maxwell fluid at low and high frequencies, displaying exclusively shear thinning across a wide range of densities and activities. Remarkably, the cross-over point between the storage and loss moduli is non-monotonic, rising with activity before the MIPS transition but falling with activity after the transition, revealing the subtleties of how active forces and intrinsically out-of-equilibrium phases affect the mechanical properties of these systems.

Active materials, composed of self-propelled units that consume energy to generate motion, display a variety of fascinating properties that deviate from those of systems at equilibrium [1, 2]. This includes large correlated motion [3, 4], anomalous transport [5–9], and emergent self-organization [8, 10–12]. Motility-Induced Phase Separation (MIPS), where a solution of motile particles separates into co-existing dense and dilute regions in the absence of any attractive interactions, is a textbook example of a behavior that is exclusive to active systems [13]. The origin of the MIPS transition and how it depends on the details of the particle interactions has been the subject of intense scrutiny [14–19]. This is because active Brownian particles (ABP) represent the simplest active model with a well-defined interplay between thermal, dispersion and active forces [20]. The intrinsically out-of-equilibrium nature of the self-organized structures in MIPS implies that traditional approaches and even definitions that are workhorses in the context of equilibrium statistical mechanics must be applied with care. Striking examples are studies using different (and conflicting) definitions of surface tension to characterize the statistical properties of the dense-fluid MIPS interface [21–30].

Despite standing as possibly one of the most fundamental active states of matter, the mechanical properties of the MIPS phase remain poorly understood, especially its response to external driving forces. Much of the previous work on externally driven ABPs has focused on very dense or crystalline suspensions in which activity can fluidize an otherwise "jammed" sys-

tem [31], and induce either shear thinning [32] or shear thickening [33] depending on the softness of the particles. In contrast, the rheological properties of dilute ABPs, where activity drives large-scale density variations through MIPS [13], is largely unexplored. Crucially, while MIPS is often described as a liquid-gas phase separation due to its mathematical analogy with equilibrium systems [34], a significant degree of local crystalline order is detectable within the dense phase [13]. The translational symmetry breaking suggests that the dense phase is more akin to a solid crystal than a liquid droplet. This apparent paradox raises key questions about the rheological nature of such systems, since broken symmetries generally result in elasticity — at least in passive materials. Traditionally, the rheological properties of passive systems arise from a thermal relaxation in response to external driving. However, active materials behave differently because of the intrinsically out-of-equilibrium pathways by which emergent phenomena and novel behaviors can arise in response to driving forces. Notable examples of active responses to external driving include super-fluid like behavior [35], the emergence of higher-order defects [36], non-linear Darcy's law [37, 38] and negative drag [39].

While the field of active matter holds promise for developing exciting materials with unusual mechanical properties, understanding how these materials respond to external driving forces is key to comprehending, controlling and designing their mechanical behavior. Studying the rheology of the MIPS phase is a first fundamental step in this direction. In this work, we

study the rheological behavior of a suspension of pseudo-hard ABPs across the MIPS transition using numerical simulations. We consider both oscillatory and steady shear, and gain new insight into the unusual mechanical properties of the MIPS state. We show that the rheological response is akin to a Maxwell fluid at low and high frequencies, but has an extended crossover regime at intermediate frequencies. Furthermore, we discover that the crossover point is non-monotonic with activity since the timescale switches from one associated with the thermal component of the individual active particles to one associated with their active persistent motion.

We perform Brownian dynamics simulations of N ABP of diameter d in two dimensions. The equations of motion for the position \mathbf{r}_i and orientation $\mathbf{n}_i = [\cos(\theta_i), \sin(\theta_i)]$ of particle i are given by

$$\frac{d\mathbf{r}_i}{dt} = -\frac{1}{\zeta} \nabla U_i + v_0 \mathbf{n}_i + \sqrt{2D_T} \boldsymbol{\xi}_i \quad (1a)$$

$$\frac{d\theta_i}{dt} = \sqrt{2D_R} \xi_i \quad (1b)$$

where ζ is the translational friction coefficient, $U_i = \sum_{j \neq i}^N U_{ij}$ is the total pairwise potential for particle i , v_0 is the self-propulsion speed of the particle, D_T is the translation diffusion, $D_R = 3D_T/d^2$ the rotation diffusion and $\boldsymbol{\xi}_i$ is the white Gaussian noise with $\langle \boldsymbol{\xi}_i \rangle = \mathbf{0}$; $\langle \boldsymbol{\xi}_i(t) \otimes \boldsymbol{\xi}_j(t') \rangle = \mathbf{1} \delta_{ij} \delta(t - t')$. The self-propulsion speed can be imagined as due to an active force of strength $F_a = \zeta v_0$. We resolve the equations of motion using LAMMPS [40]. The excluded volume interaction between the particles is enforced via the pairwise pseudo-hard sphere potential [41]

$$U_{ij} = \begin{cases} \epsilon 50 \left(\frac{50}{49}\right)^{49} \left[\left(\frac{d}{r_{ij}}\right)^{50} - \left(\frac{d}{r_{ij}}\right)^{49} \right] + \epsilon, & r_{ij} < \frac{50}{40} d \\ 0, & \text{otherwise} \end{cases} \quad (2)$$

where r_{ij} the interparticle distance and ϵ the characteristic energy of the system with Lennard-Jones units. Throughout this work, we used dimensionless units, with $\epsilon = 1$, $d = 1$ and the time unit $\tau = 1$. Since at equilibrium the potential reproduces the second virial coefficient of hard spheres when the temperature is $k_B T = 1.5\epsilon$ [41], we set $T = 1.5$, which gives $D_T = 1.5$ and $D_R = 4.5$. The rest side length of the simulation box is $L_x = L_y = 100$, and the number of particles is obtained from the number density, $\rho = 0.5$ unless otherwise stated.

While the system undergoes strain deformations, Lees-Edwards boundary conditions are applied [42, 43]. We use a strain that does not impart any torque on the orientation of the particles (inclusion of such torque does not change the reported behavior [32, 44, 45]). When a strain γ with strain rate $\dot{\gamma}$ is applied to the active system, the dynamics of individual particles are governed by two dimensionless numbers Pe_s and Pe_a [33]. The

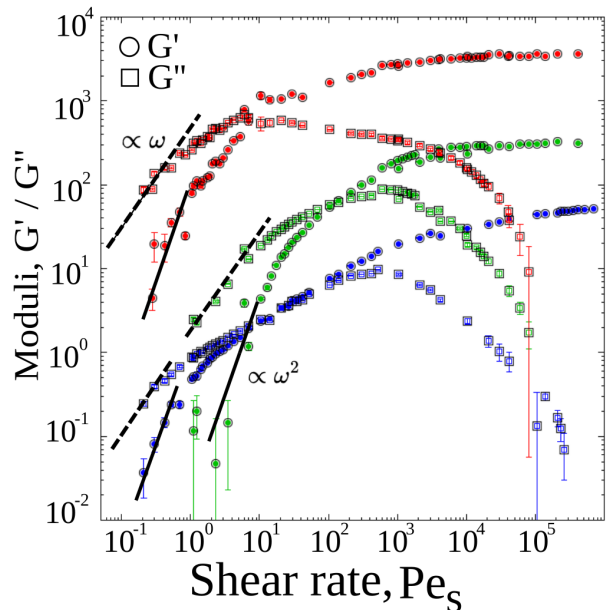


FIG. 1. Storage moduli G' (closed circles) and loss moduli G'' (open squares) with oscillation amplitude $A_x/L_y = 5\%$ (SAOS regime) for $\rho = 0.5$ and different activities $\text{Pe}_a = 0$ (blue), 42 (green) and 120 (red). Dashed and straight lines are visual guides to show the expected maxwell scaling of ω^1 and ω^2 .

shear Péclet number

$$\text{Pe}_s = \frac{\dot{\gamma} d^2}{D_T} \quad (3)$$

provides information about the relevance of the imposed shear rate with respect to thermal fluctuations, while the Active Péclet number

$$\text{Pe}_a = \frac{3v_0}{D_R d} \quad (4)$$

measures the ratio between the orientation decorrelation time $\tau_R = 1/D_R$ and self-propulsion time $\tau_a = d/v_0$.

The stress response to strain deformations is calculated as

$$\boldsymbol{\sigma} = -\frac{1}{2L_x L_y} \sum_{i=1}^N \sum_{i>j} \frac{\partial U}{\partial \mathbf{r}_{ij}} \frac{\mathbf{r}_{ij} \otimes \mathbf{r}_{ij}}{r_{ij}}, \quad (5)$$

which gives the virial contribution due to interparticle interactions (**Eq. 2**). "Swimming" stress, which is the self-propelled contribution [46–48], is not taken into account because the orientations are decoupled from the shear flow in these simulations, such that off-diagonal terms average to zero [32, 33, 44].

If the amplitude of the applied deformation is sufficiently small, the system responds linearly with stress proportional to strain, $\gamma(t) = (A_x/L_y) \sin(\omega t)$, and strain rate, $\dot{\gamma}(t) = (A_x \omega/L_y) \cos(\omega t)$, where ω is the frequency of the oscillatory shear. In this regime, only

the first-order natural modes of the system are excited [49, 50], corresponding to the Small Amplitude Oscillatory Shear (SAOS) regime and the resulting stress response is

$$\sigma_{xy}(t) = G'\gamma(t) + G''\omega\dot{\gamma}(t), \quad (6)$$

where G' and G'' are the storage and loss moduli, respectively. To ensure that the response of the system remains linear with applied deformation, an amplitude sweep at fixed frequency is performed to identify the range of amplitudes for which G' and G'' are independent of the strain amplitude (SI [51]). We find that $A_x/L_y = 5\%$ ensures that the system operates within the linear regime across a broad range of frequencies while providing a sufficiently high measurable response.

Figure 1 shows the interplay between the elastic, G' , and viscous, G'' , responses of the system for different values of Pe_a , and includes data below (blue), above (red) and at (green) the MIPS transition (see SI [51]). Interestingly, regardless of Pe_a , the system shows a liquid-like response ($G'' > G'$) at low frequencies (small Pe_s). This is an expected result for the passive system which is characterized by a single low density fluid phase (blue data). However, the behavior above the MIPS transition point (red data) indicates that the elastic response is still compatible with that of a liquid rather than that of a solid, despite the high degree of crystalline order observed within the fully formed condensed phase (**Fig. 2**; inset). This result is not expected for passive materials and suggests that non-insignificant particle rearrangement occurs within the active condensed clusters under the action of low-frequency shear forces. As the frequency increases from low Pe_s , both moduli increase. For the systems in this regime, $G'' \sim \omega$ and $G' \sim \omega^2$. Interestingly, these exponents are precisely what one would expect for a Maxwell fluid in the low frequency limit [52].

At high frequencies (large Pe_s), the storage modulus G' approaches a plateau (**Fig. 1**). This is independent of Pe_a and occurs for both the passive and the active systems. Simultaneously, the loss modulus G'' is drastically reduced as the oscillation period becomes much shorter than the typical relaxation time, causing the system to behave as a purely elastic solid for small amplitudes. In this regime, the deformation of the system and the displacement of the particles are synchronized, resulting in the loss modulus $G'' \rightarrow 0$. This too is what one expects for a Maxwell fluid.

Since both moduli increase at low frequencies, with G' rising faster than G'' , the curves meet at a crossover point, Pe_s^\dagger , which establishes the dominant relaxation time of the material ($\sim 1/Pe_s^\dagger$), and the onset value above which the system exhibits an elastic (solid-like) response against the external shear forces. For the passive system ($Pe_a = 0$), the crossover occurs at a shear rate of $Pe_s^\dagger \simeq 30$ (**Fig. 2**). As activity is introduced,

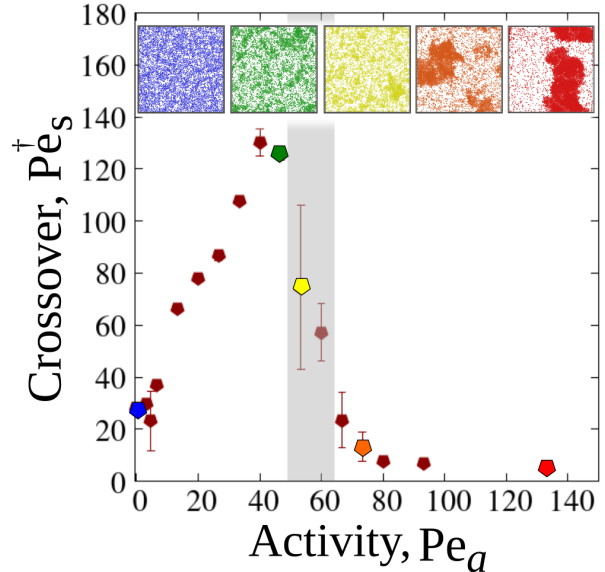


FIG. 2. Dimensionless crossover frequency Pe_s^\dagger for storage G' and loss G'' moduli shown in **Fig. 1** as a function of dimensionless activity Pe_a at density $\rho = 0.5$ for oscillation amplitude $A_x/L_y = 5\%$ (SAOS regime). Shaded area represents the MIPS phase separation boundary of the state diagram (see SI [51]). **Insets:** Snapshots of the system for the colored point at different activities.

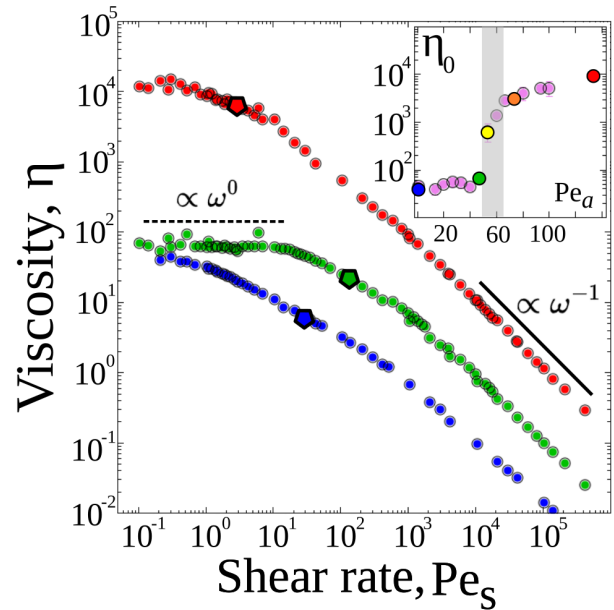


FIG. 3. Effective viscosity η as a function of the dimensionless frequency Pe_s with oscillation amplitude $A_x/L_y = 5\%$ (SAOS regime) for density $\rho = 0.5$ and different activities: $Pe_a = 0$ (blue), 42 (green) and 120 (red). All data points computed from **Fig. 1** using **Eq. 7**. **Inset:** Zero-shear limit of effective viscosity $\eta_0 = \lim_{Pe_s \rightarrow 0} \eta$ as a function of the activity. Colored points follows same color code as in **Fig. 2**

Pe_s^\dagger increases with Pe_a until it reaches a maximum right before the MIPS transition point where the suspension

begins to phase separate. At the transition point, a sharp drop in Pe_s^\dagger occurs, which eventually saturates to $Pe_s^\dagger \simeq 5$ at high activities once large clusters develop within the suspension.

The non-monotonic behavior of the crossover point stresses the non-equilibrium nature of the MIPS transition. Before the system phase separates, the active forces effectively increase the fluidity of the gas rather than promoting rigidity as we approach the MIPS transition. The linear growth of Pe_s^\dagger with the activity, points to the active timescale $\tau_a = d/v_0$ as the most relevant characteristic time for the response in this regime.

It is tempting to associate the role of activity in this gas-like regime with a factor that increases an effective temperature of the system, but the nature of the transition is more subtle. Indeed, as the system crosses the MIPS transition, particles begin to aggregate into clusters. This is because their rotational diffusion time $\tau_r = 1/D_R$ determines the rate at which particles can escape the surface of these clusters [53, 54]. Contrary to the previous case, in this regime activity takes the role of an effective attraction that drives the formation of dense clusters and τ_r becomes the relevant timescale for the system response, as indicated by the constant value of Pe_s^\dagger above the MIPS transition (**Fig. 2**).

Together, these considerations explain why MIPS responds like a Maxwell fluid, with a single characteristic time scale at low and high frequencies, but with a non-monotonic crossover point which depends on activity: At low activities (in the gas-like phase below MIPS), it is the active time scale τ_a that dominates the response and so Pe_s^\dagger grows linearly with $Pe_a \sim v_0$. At the MIPS transition, the system begins to phase separate and the crossover point drops sharply to a value $Pe_s^\dagger \simeq 5$ that is independent of activity because the system is dominated by the presence of large clusters and the relaxation time associated with the clusters is τ_r , which now sets the crossover point, independent of activity. The presence of the dense clusters and the purely thermal nature of τ_r , explain the drop in value of Pe_s^\dagger and its independence of Pe_a . While the low and high frequency limits are dominated by single timescales, the response at intermediate frequencies around the crossover Pe_s^\dagger is more complex, exhibiting an extended regime compared to Maxwell fluids (**Fig. 1**). While the low and high-frequency limits scale like a simple Maxwell-like fluid, the crossover cannot be captured with a single timescale and so the moduli cannot be fit to a single Maxwell fluid across all frequencies.

Overall, the behavior of the G'/G'' as shown in **Fig. 1** and that of Pe_s^\dagger in **Fig. 2** suggests that suspensions of ABPs both below and above the MIPS transition have a fairly simple response akin to a Maxwell fluid. A Maxwell model of a fluid is characterized by a constant complex viscosity at low frequencies and shear thinning at high frequencies. To further explore this analogy,

we next extract the effective shear viscosity of the ABP system using

$$\eta = \sqrt{\left(\frac{G'}{\omega}\right)^2 + \left(\frac{G''}{\omega}\right)^2}. \quad (7)$$

This definition has been previously employed to uncover non-trivial behavior in various active systems, ranging from increasing viscosity with activity to negative viscosities [55–57].

Pseudo-hard ABPs show that the zero-frequency limit of the viscosity does not increase above the passive values (**Fig. 3**; blue and green curves). A clear transition from Newtonian to shear-thinning behavior is observed as Pe_s increases, when a marked decay of the viscosity is observed. The zero-frequency limit of the viscosity is constant until the MIPS transition, at which point it suddenly begins to rise (**Fig. 3**; inset). For this low activity limit, additional activity broadens the range over which the suspension maintains Newtonian-like behavior with a constant viscosity (**Fig. 3**; green). The situation is different above the MIPS transition (**Fig. 3**; red), where the zero-frequency viscosity is significantly larger than that of the passive system, suggesting that MIPS clusters enhance viscous dissipation. Furthermore, the shear thinning onset above the MIPS transition occurs at frequencies that are smaller than those of the active suspensions below the MIPS transition, effectively reducing the Newtonian range. At sufficiently large shear (Pe_s), all curves exhibit a characteristic thinning behavior, with the viscosity decaying proportionally as $\eta \sim Pe_s^{-1} \sim \omega^{-1}$. This decay arises at high frequencies because $G' \gg G''$ and the storage modulus remains roughly constant, leading to the scaling $\eta \approx G'/\omega \sim \omega^{-1}$. This result has been previously observed in other active systems [32, 58].

To further investigate the shear-thinning behavior observed in the high-frequency limit, we use non-linear constant shear measurements. Under constant shear, at high rates the shear response excites higher order modes. For Pe_s beyond the cross-over point, the stress follows a simple power law (**Fig. 4a**) which is characterized using the Herschel-Bulkley model [59]

$$\sigma_{xy} = A + B\dot{\gamma}^n. \quad (8)$$

A Herschel-Bulkley exponent n smaller than 1 is indicative of shear-thinning behavior, while $n > 1$ is associated to shear thickening and $n = 1$ corresponds to a classical Newtonian fluid. Figure 4b shows the Herschel-Bulkley exponent n obtained by fitting our numerical data to the Herschel-Bulkley model for different values of the active Péclet number at a fixed density $\rho = 0.5$. The inset shows n at a fixed active force, $Pe_a = 120$, as a function of the system density ρ (see SI [51]). Crucially, the power decreases monotonically with both parameters and is systematically less than 1, indicating shear-thinning behavior at high frequencies for all activities

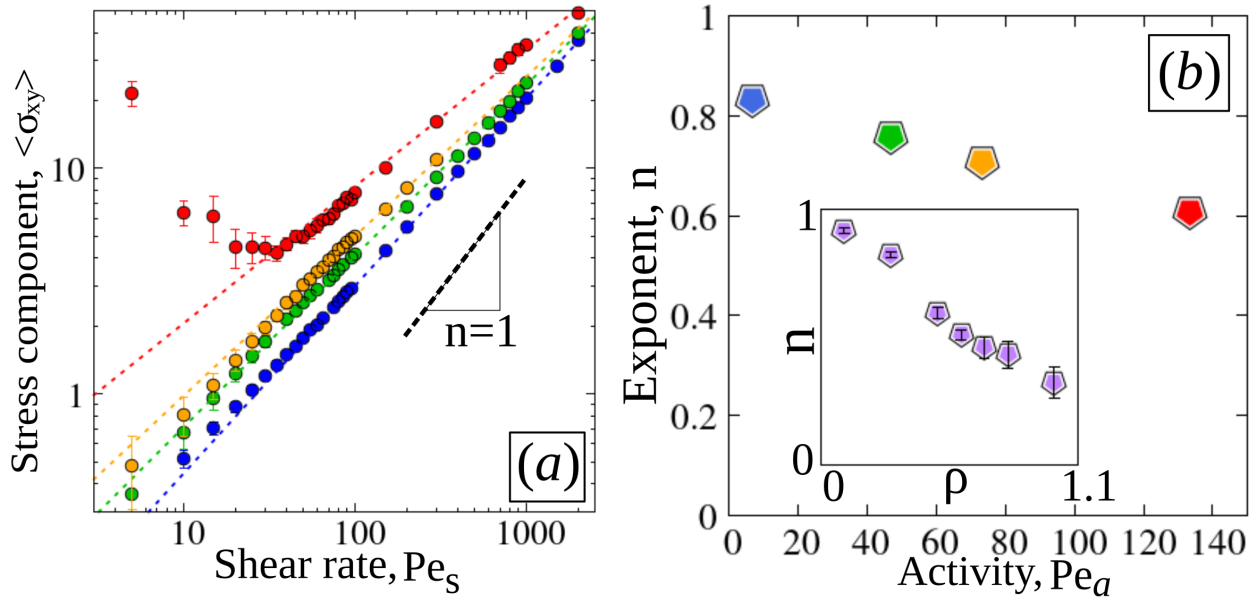


FIG. 4. (a) Average out-of-diagonal stress component $\langle \sigma_{xy} \rangle$ for simulations with constant shearing as a function of dimensionless shear rate Pe_s for density $\rho = 0.5$ and dimensionless activities $Pe_a = 6$ (blue), 42 (green), 66 (orange) and 120 (red). (b) Power law exponents for the curves shown in panel (a) as a function of dimensionless activity Pe_a for $\rho = 0.5$. **Inset:** The dependency of the exponent n on density ρ for $Pe_a = 120$.

and densities. This result suggests that increased activity in ABP suspensions enhances fluidization both below and above the MIPS transition. Consequently, this leads to a decrease in the shear-thinning exponent as activity increases.

Previous studies on the rheology of active colloidal particles under constant shear have reported shear-thickening behavior [32, 33]. However, these found shear thickening only for high shear rates and extreme densities [33]. The primary differences between our results and previous studies is that previous studies focus exclusively on soft overlapping particles at densities well above that of closed-packed disks, while we consider the effect of shear forces on pseudo-hard ABP across the MIPS transition.

While previous studies have considered the phase behavior of MIPS and proposed useful analogies to co-existence in passive liquid-liquid phase separation [60], the study presented here has considered the rheological response of MIPS for the first time. The results have revealed a rheological analogy: MIPS responds like a Maxwell fluid at low and high frequencies, but has an extended crossover regime at intermediate frequencies and a non-monotonic crossover point that follows the active timescale below the MIPS transition and the rotational relaxation timescale above. In addition to demonstrating how rheological measurements can be used by future studies to reveal more about self-assembled structures in intrinsically out-of-equilibrium materials, these findings show that even simple realizations of activity can result in complex and exciting rheological responses since

active materials possess alternative routes to respond beyond the thermodynamically accessible pathways of purely passive materials.

ACKNOWLEDGEMENTS

This research has received funding (T.N.S. and K.T.) from the European Research Council under the European Union's Horizon 2020 research and innovation programme (Grant Agreement Nos. 851196 and 101029079). This work was further supported (K.T.) by the Novo Nordisk Foundation grants no. NNF18SA0035142 and NNF23OC0085012. J.M.R. acknowledges financial support from the UCM predoctoral contract (call CT15/23). C.V. acknowledges fundings IHRC22/00002 and PID2022-140407NB-C21 from MINECO. We acknowledge useful discussions with Marco Mazza and James Richards. For the purpose of open access, the author has applied a Creative Commons Attribution (CC BY) licence to any Author Accepted Manuscript version arising from this submission. The authors thank the Nordita Institute, since the idea of the project was originated during the "Current and Future Themes in Soft and Biological Active Matter" workshop.

* cvaleriani@ucm.es

† t.shendruk@ed.ac.uk

- ‡ ac2822@columbia.edu
- [1] S. Ramaswamy, *Journal of Statistical Mechanics: Theory and Experiment* **2017**, 054002 (2017).
 - [2] C. Bechinger, R. Di Leonardo, H. Löwen, C. Reichhardt, G. Volpe, and G. Volpe, *Reviews of Modern Physics* **88**, 045006 (2016).
 - [3] P. Baconnier, O. Dauchot, V. Démery, G. Düring, S. Henkes, C. Huepe, and A. Shee, *Reviews of Modern Physics* **97**, 015007 (2025).
 - [4] S. A. Mallory, C. Valeriani, and A. Cacciuto, *Annual Review of Physical Chemistry* **69**, 59 (2018).
 - [5] S. Williams, R. Jeanneret, I. Tuval, and M. Polin, *Nature Communications* **13**, 4776 (2022).
 - [6] Z. Liao, M. Han, M. Fruchart, V. Vitelli, and S. Vaikuntanathan, *The Journal of Chemical Physics* **151** (2019).
 - [7] J. Martín-Roca, C. M. Barriuso G, R. Martínez Fernández, C. Betterelli Giuliano, R. Zhang, C. Valeriani, and L. G. Wilson, *Proceedings of the National Academy of Sciences* **122**, e2409510121 (2025).
 - [8] O. Granek, Y. Kafri, and J. Tailleur, *Physical Review Letters* **129**, 038001 (2022).
 - [9] N. Koumakis, C. Maggi, and R. Di Leonardo, *Soft Matter* **10**, 5695 (2014).
 - [10] S. Ramaswamy, *Annual Review of Condensed Matter Physics* **1**, 323 (2010).
 - [11] S. Rana, M. Samsuzzaman, and A. Saha, *Soft Matter* **15**, 8865 (2019).
 - [12] Z. Peng and R. Kapral, *Soft Matter* **20**, 1100 (2024).
 - [13] M. E. Cates and J. Tailleur, *Annual Review of Condensed Matter Physics* **6**, 219 (2015).
 - [14] A. Torres-Carbaljal and F. J. Sevilla, *Physics of Fluids* **36** (2024).
 - [15] J. Martín-Roca, R. Martinez, L. C. Alexander, A. L. Diez, D. G. Aarts, F. Alarcon, J. Ramirez, and C. Valeriani, *The Journal of Chemical Physics* **154** (2021).
 - [16] J. Stenhammar, D. Marenduzzo, R. J. Allen, and M. E. Cates, *Soft Matter* **10**, 1489 (2014).
 - [17] T. Kolb and D. Klotsa, *Soft Matter* **16**, 1967 (2020).
 - [18] M. E. Cates and J. Tailleur, *Europhysics Letters* **101**, 20010 (2013).
 - [19] A. P. Solon, J. Stenhammar, R. Wittkowski, M. Kardar, Y. Kafri, M. E. Cates, and J. Tailleur, *Physical Review Letters* **114**, 198301 (2015).
 - [20] M. C. Marchetti, Y. Fily, S. Henkes, A. Patch, and D. Yllanes, *Current Opinion in Colloid & Interface Science* **21**, 34 (2016).
 - [21] J. Bialke, J. Siebert, H. Lowen, and T. Speck, *Physical Review Letters* **115**, 098301 (2018).
 - [22] A. Patch, D. M. Sussman, D. Yllanes, and M. Marchetti, *Soft Matter* **14**, 7435 (2018).
 - [23] A. Omar, Z.-G. Wang, and J. Brady, *Physical Review E* **101**, 012604 (2020).
 - [24] J. T. Siebert, F. Dittrich, F. Schmid, K. Binder, T. Speck, and P. Virnau, *Physical Review E* **98**, 030601 (2018).
 - [25] F. Ginot, I. Theurkauff, D. Levis, C. Ybert, L. Bocquet, L. Berthier, and C. Cottin-Bizonne, *Physical Review X* **5**, 011004 (2015).
 - [26] Y. Fily, A. Baskaran, and M. F. Hagan, *Soft Matter* **10**, 5609 (2014).
 - [27] S. C. Takatori, W. Yan, and J. F. Brady, *Physical Review Letters* **113**, 1 (2014).
 - [28] S. A. Mallory, A. K. Omar, and J. F. Brady, *Physical Review E* **104**, 044612 (2021).
 - [29] E. Chacón, F. Alarcón, J. Ramírez, P. Tarazona, and C. Valeriani, *Soft Matter* **18**, 2646 (2022).
 - [30] S. Hermann, D. de las Heras, and M. Schmidt, *Physical Review Letters* **123**, 268002 (2019).
 - [31] S. Ongena, M. Cuvelier, J. Vangheel, H. Ramon, and B. Smeets, *Frontiers in Physics* **9**, 649821 (2021).
 - [32] R. Wiese, K. Kroy, and D. Levis, *Phys. Rev. Lett.* **131**, 178302 (2023).
 - [33] A. G. Bayram, F. J. Schwarzendahl, H. Löwen, and L. Biancofiore, *Soft Matter* **19**, 4571 (2023).
 - [34] L. Hecht, I. Dong, and B. Liebchen, *Nature Communications* **15**, 3206 (2024).
 - [35] S. Takatori and J. Brady, *Physical Review Letters* **118**, 018003 (2017).
 - [36] D. P. Rivas, T. N. Shendruk, R. R. Henry, D. H. Reich, and R. L. Leheny, *Soft Matter* **16**, 9331 (2020).
 - [37] F. Mackay, J. Toner, A. Morozov, and D. Marenduzzo, *Physical Review Letters* **124**, 187801 (2020).
 - [38] R. R. Keogh, T. Kozhukhov, K. Thijssen, and T. N. Shendruk, *Physical Review Letters* **132**, 188301 (2024).
 - [39] G. Foffano, J. S. Lintuvuori, K. Stratford, M. E. Cates, and D. Marenduzzo, *Physical Review Letters* **109**, 028103 (2012).
 - [40] A. P. Thompson, H. M. Aktulga, R. Berger, D. S. Bolintineanu, W. M. Brown, P. S. Crozier, P. J. in 't Veld, A. Kohlmeyer, S. G. Moore, T. D. Nguyen, R. Shan, M. J. Stevens, J. Tranchida, C. Trott, and S. J. Plimpton, *Computer Physics Communications* **271**, 108171 (2022).
 - [41] J. Jover, A. Haslam, A. Galindo, G. Jackson, and E. Müller, *The Journal of Chemical Physics* **137**, 144505 (2012).
 - [42] A. Lees and S. Edwards, *Journal of Physics C: Solid State Physics* **5**, 1921 (1972).
 - [43] M. P. Allen and D. J. Tildesley, *Computer simulation of liquids* (Oxford university press, 2017).
 - [44] R. Mandal and P. Sollich, *Proceedings of the National Academy of Sciences* **118**, e2101964118 (2021).
 - [45] C. Villarroel and G. Düring, *Soft Matter* **17**, 9944 (2021).
 - [46] R. G. Winkler, A. Wysocki, and G. Gompper, *Soft Matter* **11**, 6680 (2015).
 - [47] S. C. Takatori, W. Yan, and J. F. Brady, *Physical Review Letters* **113**, 028103 (2014).
 - [48] Y. Hatwalne, S. Ramaswamy, M. Rao, and R. A. Simha, *Physical Review Letters* **92**, 118101 (2004).
 - [49] H. A. Barnes, J. F. Hutton, and K. Walters, *An introduction to rheology*, Vol. 3 (Elsevier, 1989).
 - [50] U. Daalkhaijav, (2018).
 - [51] See Supplemental Material at URL-will-be-inserted-by-publisher.
 - [52] M. Grimm, S. Jeney, and T. Franosch, *Soft Matter* **7**, 2076 (2011).
 - [53] A. K. Omar, Y. Wu, Z.-G. Wang, and J. F. Brady, *ACS nano* **13**, 560 (2018).
 - [54] M. C. Pedersen, S. Mukherjee, A. Doostmohammadi, C. Mondal, and K. Thijssen, *Physical Review Letters* **133**, 228301 (2024).
 - [55] D. Saintillan, *Experimental Mechanics* **50**, 1275 (2010).
 - [56] S. Heidenreich, S. Hess, and S. H. Klapp, *Physical Review E* **83**, 011907 (2011).
 - [57] J. Jara, F. Alarcón, A. K. Monnappa, J. I. Santos, V. Bianco, P. Nie, M. P. Ciamarra, Á. Canales, L. Dinis, I. López-Montero, *et al.*, *Frontiers in microbiology*

- 11**, 588884 (2021).
- [58] M. Tennenbaum, Z. Liu, D. Hu, and A. Fernandez-Nieves, *Nature Materials* **15**, 54 (2016).
- [59] P. Saramito, *Complex fluids* (Springer, 2016).
- [60] A. K. Omar, H. Row, S. A. Mallory, and J. F. Brady, *Proceedings of the National Academy of Sciences* **120**, e2219900120 (2023).